Prefailure Damage Processes in Highly Filled Glass/Mica/Epoxy Composites

M. REGOLA,* E. BAER,† and A. HILTNER

Department of Macromolecular Science, Case Western Reserve University, Cleveland, Ohio 44106

SYNOPSIS

In the present study, the prefailure damage processes of a series of short glass fiber/mica/epoxy composites under three-point bending were elucidated using acoustic emission (AE) coupled with *in situ* scanning electron microscopy (SEM) observations. This study consisted of a detailed investigation of the damage tolerance of composite systems that had constant inorganic content of 75% by weight with a varying ratio of glass fibers to mica. The flexural strength was found to increase from 11 to 21 ksi as the glass fiber content increased (mica content decreased), while the flexural modulus decreased from 5.0 to 2.5 Msi. By monitoring the AE during flexural deformation of the glass fiber-to-mica ratio composites, it was determined that low amplitude (0–42 db) AE events, which occurred throughout the deformation process, were caused by matrix cracking, whereas the high-amplitude (43–100 db) AE events, which occurred just prior to failure, were caused by a fiber-related mechanism. *In situ* SEM observations of the composites during flexural deformation allowed a correlation between the AE and the damage mechanisms as a function of strain. In the all-mica composite, microcracking initiated in the linear region at preexisting flaws, on the order of 10 μm, located at the mica interface. These microcracks grew along the mica contours over the majority of the deformation process, emitting low-amplitude events, until final fracture occurred at relatively low strains. In the glass fiber-containing composites, microcracking initiated in the linear region at preexisting flaws and voids, on the order of 10 μm. These microcracks grew slowly, emitting low-amplitude events, as the strain increased, but were prevented from causing failure at low strains because of the toughening effect of the glass fibers. At sufficiently high strains, however, fiber breakage and fiber pull-out occurred that corresponded to the high-amplitude events detected by the AE. At strains just prior to failure, catastrophic crack growth occurred, producing a rapid increase in both low- and high-amplitude events, causing ultimate failure.

INTRODUCTION

Composites are finding increased usage as structural components, oftentimes replacing materials in which the damage and failure mechanisms are well understood. Since damage accumulation in composites is closely related to the actual strength, stiffness, and life of the materials, understanding of the failure mechanisms and damage accumulation are of utmost importance.[1] This, however, has proved difficult since the failure mechanisms are quite often very complex and interrelated.

Continuous fiber–epoxy composites have received an immense amount of attention in the literature because of their structural uses. These structural uses are, in part, due to the varied processing techniques, such as hand lay-up, filament winding, and pultrusion, which are available. Although the optimum processing technique is imperative to the successful use of these materials, even more critical is an understanding of their failure mechanisms. The evaluation of the composite breakdown can be achieved in a variety of ways. One of the most useful techniques is acoustic emission (AE), as it is nondestructive. Li and Zhao studied the damage growth processes in glass fiber-reinforced composites by

* Present address: Lord Corporation, 2000 West Grandview Blvd, Erie, PA 16514.

† To whom correspondence should be addressed.

Journal of Applied Polymer Science, Vol. 42, 2563–2577 (1991)
 CCC 0021-8995/91/092563-15$04.00

conducting tensile tests on four kinds of particular-designed specimens and using AE amplitude distribution analysis.[2] At low loading levels, matrix cracking-producing low-amplitude events were found to occur. At intermediate loading levels, debonding occurs and produces a wide amplitude distribution. Finally, at high loading levels, delamination and fiber breakage occurs, producing high amplitudes. Sato et al. investigated the fracture mechanism of a unidirectional carbon–fiber reinforced epoxy resin by monitoring the AE during three-point bending tests coupled with *in situ* SEM observations of the failure process in the same load range.[3] They found a close correlation between the AE amplitudes and crack formation. Furthermore, the low-amplitude AE occurred throughout the deformation process and corresponded to delamination.

Short fiber-thermoset materials are widely used as engineering materials, most notably in the form of sheet molding compound (SMC) and bulk molding compound (BMC) composites. Faudree et al. characterized the failure and fracture mechanisms in BMCs by monitoring the AE generated during tensile tests and coupled with SEM observations of strained and fractured specimens.[4] He found two damage mechanisms that produced amplitude peaks at 40 and 70 db. The 40 db peak was associated with small microcracks that initiated at fiber and filler particles at low strains and continued until fracture. The higher-amplitude range was observed at higher strains and was associated with the small cracks coalescing into larger cracks that were spanned by pulled-out fibers.

Berthelot and Rhazi studied the AE amplitude distributions in glass fiber–polyester and glass fiber–polyamide composites during three-point flexural tests.[5] Two damage mechanisms, monitorable with amplitude distributions, were found. They consisted of an initiation phase characterized by microcracking and a damage propagation phase with localized advance of damaging processes.

In the present study, the prefailure damage mechanisms of short glass/mica/epoxy composites under three-point bending were studied using AE coupled with *in situ* SEM observations. This investigation consisted of an optimization study of the formulation variables and a detailed study of the damage tolerance of the optimized composites. The total inorganic content of the compression molded composites was optimized with respect to the flexural properties and thermal stability. The detailed investigation of the damage tolerance of the optimized composites allowed characterization and identification of the damage mechanisms leading to failure.

EXPERIMENTAL

Processing of the Composites

The composite materials in this study, which were formulated and fabricated in-house, are composed of a resin system and two different reinforcements and are shown in Tables I and II. The resin system is a bifunctional epoxy obtained from The Dow Chemical Company and designated DER332. This is cured with nadic methyl anhydride (NMA) manufactured by the Buffalo Color Corporation, and catalyzed with benzyl–dimethyl amine (BDMA) supplied by Arsynco Inc. The reinforcements were $\frac{1}{4}$ in.-length S-glass fiber #463 supplied by Owens Corning and wet ground mica manufactured by KMG Minerals Inc. A silane coupling agent (Z6040 from Dow Corning Corp.) was used to promote fiber adhesion.

The DER332, NMA, and BDMA were combined in a ratio of 100 : 85 : 3, which is the recommended ratio by Dow,[6] and dissolved into acetone along with the coupling agent. The glass fibers and mica were dried under vacuum at 180°C for 24 h. The mica and glass fibers were then mixed in a Processall, model number 4HV, manufactured by Processall Inc. This is a mixing unit containing two blades that rotate on axis perpendicular to one another. The main blade was used on its "low" setting of 200 rpm for 2 min while the small milling blade was pulsed at 50% power every few seconds. The resin solution

Table I Variable Inorganic Content Formulations (Inorganic Content by Weight)

	Formulation (% glass/% mica)			
Material	15/50	15/55	15/60	15/65
D.E.R. 332	18.62	15.96	13.30	10.64
NMA	15.82	13.56	11.30	9.04
BDMA	0.56	0.48	0.40	0.32
1/4 in. S-glass	15.0	15.0	15.0	15.0
MICA	49.5	54.5	59.5	64.5
Silane coupling agent	0.50	0.50	0.50	0.50
Total inorganic content	65	70	75	80

Table II Variable Glass Content Formulations (75% Inorganic Content by Weight)

Material	Formulation (% glass/% mica)						
	0/75	15/60	20/55	30/45	37.25/37.25	50/25	75/0
D.E.R. 332	13.30	13.30	13.30	13.30	13.30	13.30	13.30
NMA	11.30	11.30	11.30	11.30	11.30	11.30	11.30
BDMA	0.40	0.40	0.40	0.40	0.40	0.40	0.40
1/4 in. S-glass	0.00	15.0	20.0	30.0	37.3	50.0	75.0
Mica	74.5	59.5	54.5	44.5	37.2	24.5	0.00
Silane coupling agent	0.50	0.50	0.50	0.50	0.50	0.50	0.50
Glass fiber fraction	0.0	0.20	0.27	0.40	0.50	0.67	1.0

was added to the fiberglass and mica and hand-mixed with a spatula until the mixture appeared uniform. A vacuum unit was then interfaced with the Processall and run for approximately 2.5 h. The Processall's main and mill blades were pulsed a few times during the acetone removal to turn over the mixture. After the acetone was removed, as evidenced by a lack of odor, the unreacted mixture was stored in a desiccator at 0°C until use.

The fabrication of test bars was accomplished by compression molding 7 g of the material at elevated temperatures and pressures using a Wabash hydraulic press as recommended by Dow.[6] The cure cycle used was 2 h at 90°C with slight pressure, followed by 4 h at 165°C with 7500 psi pressure, and then demolding and postcuring for 16 h at 200°C in air.

The nomenclature used to identify the composite is to first list the glass content by weight, followed by the mica content by weight, with the balance being the epoxy by weight. For example, 75/0 indicates a composite of 75% glass by weight, 0% mica by weight, and 25% epoxy by weight.

Analysis

Thermal Behavior

The thermal conditions of low earth orbit (LEO) have been found to vary from approximately −125 to +125°C.[7] Therefore, a thermal stability of at least 200°C was required for the composites. The evaluation of the thermal stability was carried out on all the formulations using a Perkin–Elmer TGA Series 7. Two different methods were used to characterize the materials. The first method was a room temperature to 1000°C heating in air of the material at a rate of 20°C/minute. By following the weight loss of the material over the temperature range, the degradation temperature of the resin can be determined. The second method involves following the weight loss while maintaining the sample at 200°C in air for 4 h. The thermal criterion of 200°C is based on this experiment, in which a weight loss of less than 1% is considered adequate.

AE During Flexural Deformation

The formulations were tested in three-point bending using an Instron materials tester, Model 1123, according to ASTM-D790[8] with a crosshead speed of 0.1 mm/min. A span to depth ratio of 32 was chosen to minimize the contribution of shear in the measured properties.[9,10] At least seven samples of each formulation were tested, and the averages and standard deviations were calculated. Figure 1 shows the test setup, sample geometry, and relevant equations. Note that the AE sensor was placed on the surface of the sample 0.40 in. from the loading nose.

AE is defined as the stress (elastic) waves that accompany the sudden release of energy within a solid, caused, for instance, by the growth of a crack.

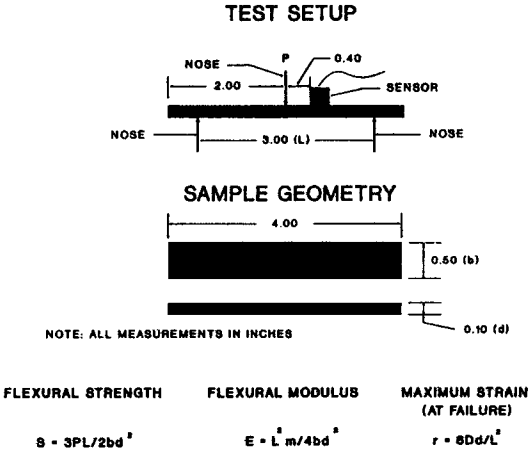

Figure 1 ASTM-D790 test setup showing the three point bend apparatus, sample geometry, and equations used.

Large and rapid stress changes, characteristic of a brittle crack, generate high-energy waves with high amplitudes, whereas ductile cracking generates lower-energy waves with lower amplitudes because of energy losses associated with the driving of dislocations in the enlarging plastic zone.[11] The common denominator in all cases is the necessity of microscopic movement, usually accomplished by the application of a macroscopic stress. This makes AE intimately related to failure processes.

Detection of the AE is accomplished by coupling transducers, which usually function by utilizing the piezoelectric effect, to the surface that are capable of detecting surface displacements on the order of picometers. This works best when the transducer is in intimate contact with the surface and is achieved by using grease or some other nonattenuating fluid as a coupling medium. The detected signal is never the same as the emitted signal due to attenuation caused by geometric spreading of the wavefront, absorption, or damping within the specimen and "leaking" of the wave energy into adjacent media.[12] Additionally, true AE signals must be differentiated from continuous background noise.

AE from composites is characterized by a series of burst emissions.[13] Each burst is called an event and corresponds to the formation or propagation of defects. Important waveform characteristics are the number of counts or events, amplitude, energy, rise time, and event duration. The number of counts, defined as the number of oscillations per burst (event), and wave energy, the area under the rectified signal, give information on the amount of damage. The amplitude of the wave is characteristic of each damage mechanism and indicates the number of different mechanisms occurring. The rise time, defined as the time from the first count to the peak amplitude count, and event duration can be used to distinguish delamination fracture as well as to eliminate noise.

When a fiber-reinforced composite is subjected to external loading, fiber fracture, matrix cracking, and debonding at the fiber-matrix interface can occur.[2,14,15,16] Acoustic emission can be used to distinguish between these mechanisms in two ways. The first involves correlation of the AE with some type of visual evidence, usually scanning electron microscopy.[3,4,14,17,18] The other method involves variation of the composition while monitoring changes in the amplitude distribution.[2,19,20] In this study, both types of analysis were employed.

A piezoelectric transducer with a resonant frequency of 150 kHz was coupled to the sample with vacuum grease as shown in Figure 1. The transducer was then fed into a PAC Spartan AT that was controlled by an Everex 386/20 computer using the PC-DAQ software program. A threshold of 28 db was used to eliminate continuous background noise.

Scanning Electron Microscopy during Flexural Deformation

As previously mentioned, SEM can be coupled with the AE to yield further insight into the damage processes. This was accomplished by *in situ* monitoring of the damage progression of the 0/75, 37.25/37.25, and 75/0 samples using a miniature three-point bend setup in a JEOL JSM-840A low-voltage SEM. The SEM test setup is shown in Figure 2. This technique allows observation in a stepwise manner of the damage process occurring on the tensile side as a function of applied strain by removing the unit, tightening the screws, and repeating until failure. The samples were polished to an L/d ratio of approximately 32 so the strains obtained would correspond to the strains obtained in the Instron/AE tests and subsequently coated with about 100 Å of gold before observation. The presence of the gold coating allowed easy observation of the underlying composite cracking because the broken coating glows in the electron beam.

Fracture surfaces were studied at predetermined locations to give further insight on the damage processes as well as information on the sample morphology. The surfaces were coated with approximately 100 Å of palladium before observation.

RESULTS AND DISCUSSION

Thermal Behavior

Figure 3 shows a typical TGA curve of weight vs. temperature for all the formulations. It is seen that the onset of the first weight drop is about 240°C,

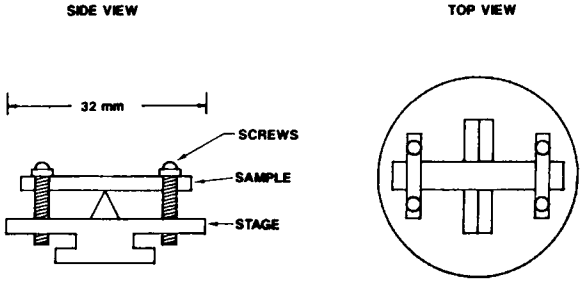

Figure 2 Three-point bend setup in the SEM.

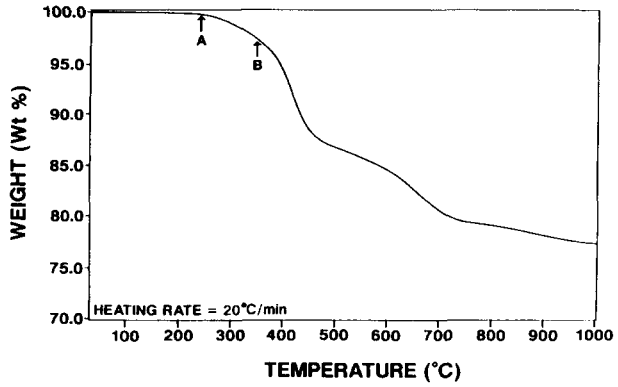

Figure 3 Typical weight vs. aging temperature (in air).

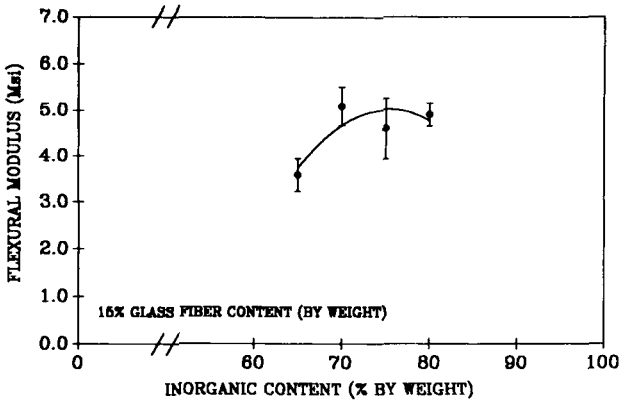

Figure 5 Flexural modulus vs. inorganic content.

whereas the point of inflection is about 350°C, indicated by point "A" and "B," respectively. Both of these temperatures are above the maximum temperature of 125°C in LEO and therefore indicate that the composites would be stable at LEO temperatures. However, as outlined in the Experimental section, the composites are considered thermally stable if a weight loss of less than 1% occurs when the materials are subjected to a temperature of 200°C for 4 h. Figure 4 shows the results of this stability experiment in which it is seen that the composites lose about 0.6% weight over 4 h at 200°C. Therefore, the composites are considered thermally stable.

Optimization of Formulation Variables

Flexural Properties

To proceed with an in-depth study of the composites, it was desirable to optimize the formulation to yield the highest mechanical properties. This was achieved by varying the total inorganic content of the composites from 65 to 80% by weight while maintaining the glass-fiber content at 15% by weight and varying the amount of mica. An initial glass-fiber loading of 15% by weight was chosen for two reasons. The first was to reduce cost since the glass fibers are substantially more expensive than is the mica, and the second was to maintain the strength as it was believed that this was the minimum amount possible. These formulations are shown in Table I.

Figures 5–7 show the results of this study. In Figure 5, the flexural modulus is seen to increase from approximately 3.5 Msi at 65% by weight total inorganic content to a plateau of about 4.8 Msi between 70 and 80% total inorganics. The flexural strength, shown in Figure 6, has a plateau of approximately 17 ksi between 70 and 75% total inorganic content with lower values at 65 and 80%. The maximum strain, shown in Figure 7, exhibits no clear correlation due to the standard deviations. This behavior is explained by a rule of mixtures approach, that is, the amount of resin present in the system. At 65% inorganic content, the samples were visibly

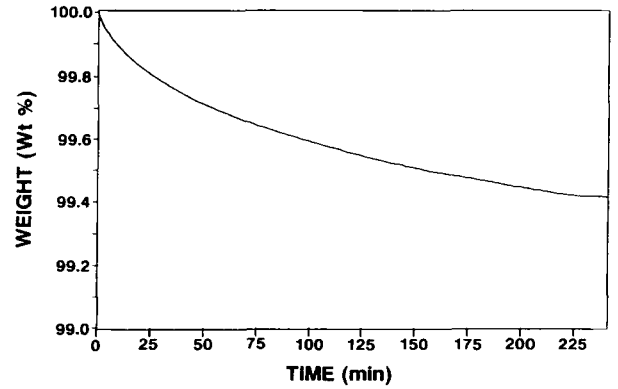

Figure 4 Typical weight vs. aging time (in air at 200°C).

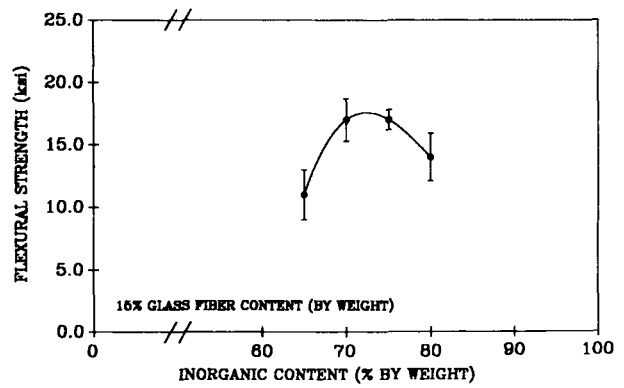

Figure 6 Flexural strength vs. inorganic content.

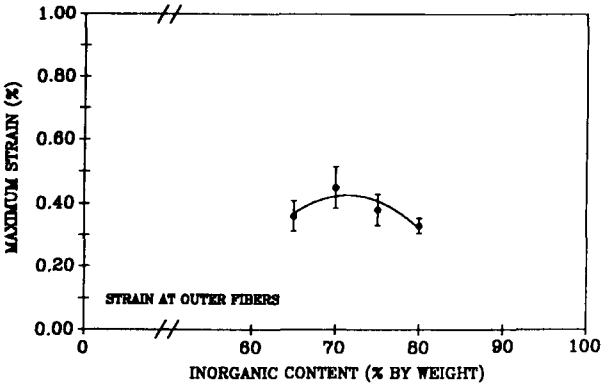

Figure 7 Maximum strain vs. inorganic content.

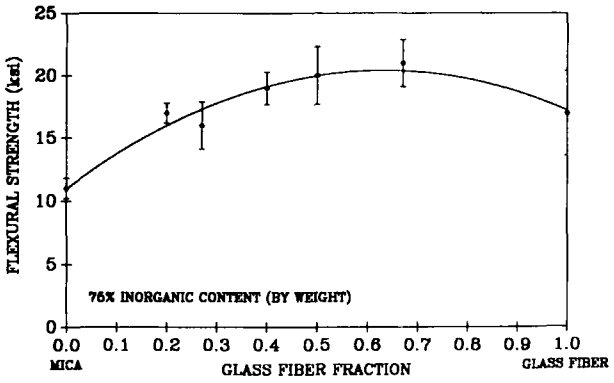

Figure 9 Flexural strength vs. glass-fiber fraction.

resin-rich. From basic composite micromechanics considerations, this causes a lowering of the properties toward the resin properties. At 80% inorganic content, the composites showed resin-poor areas, lowering the properties because of a lack of resin binding the fibers. These two effects work in opposition and yielded an optimum total inorganic content of 75% by weight.

Detailed Study of Damage Tolerance

Flexural Properties

Once this optimum inorganic content was obtained, the roles the glass fibers and mica played in the determination of properties were investigated. This was accomplished by varying the glass fiber-to-mica ratio and measuring the flexural properties. Furthermore, AE was monitored throughout the compositional range and will be discussed later. The formulations tested are shown in Table II. Note that the total inorganic content remains constant at 75% by weight. Figure 8 shows the relationship between the flexural modulus and the glass fiber/mica ratio, which is represented by the glass-fiber fraction. As can be seen, as the glass-fiber fraction decreases (glass-fiber content decreases and mica content increases), the flexural modulus increases in a linear fashion from about 2.5 Msi in the all-glass fiber composite to approximately 5.0 Msi in the all-mica composite. The effect of the glass-fiber/mica ratio on the flexural strength is shown in Figure 9. Here, the opposite effect is observed, that is, as the glass-fiber fraction increases, the flexural strength increases from about 11 ksi in the all mica composite to a high of approximately 21 ksi in the 50% glass/25% mica (50/25) composite. Note that this relationship is not linear and that the all-glass fiber composite has a slightly lower flexural strength, about 17 ksi, but a much larger standard deviation. Figure 10 shows the effect of the glass fiber/mica ratio on the maximum strain at fracture. This relationship is similar to the flexural strength in that as the glass-fiber fraction increases the maximum strain increases. Note, however, that the drop between the 50/25 composite and the 75/0 composite

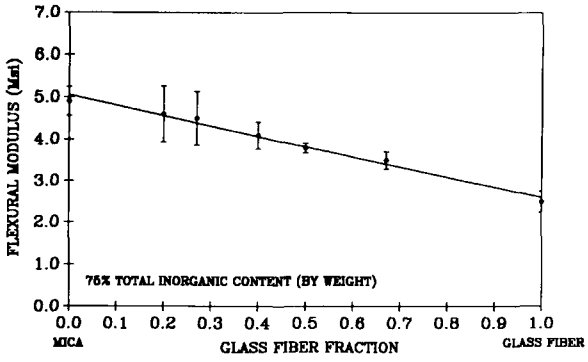

Figure 8 Flexural modulus vs. glass-fiber fraction.

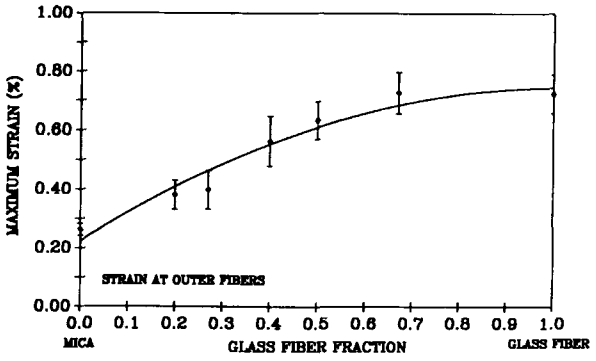

Figure 10 Maximum strain vs. glass-fiber content.

Table III Comparison of the Flexural Properties of the Glass/Mica Ratio Composites of This Study to Some Composite Systems in the Literature

Material	Flexural Modulus (Msi)	Flexural Strength (ksi)	Reference
Mica/epoxy (15/85[a])	0.93–0.97	10.0–10.3	21
Glass/polyester (22/78[a])	1.5–2.2	—	36
Glass/polyester (20/80[b])	1.3–1.6	6.2–8.9	38
Glass/polyamide (30/70[b])	1.5	44	41
Glass/mica/epoxy			
(0/75/25[b])	4.55–5.23	10.5–12.0	–
(37.25/37.25/25[b])	3.70–3.94	17.8–22.4	–
(75/0/25[b])	2.26–2.76	13.2–20.0	–

[a] Volume %.
[b] Weight %.

is much lower and is, in fact, insignificant due to the standard deviations. Table III shows a comparison of the flexural properties of the glass fiber/mica ratio composites to some similar composite systems in the literature. The flexural modulus of the glass fiber/mica ratio composites are significantly higher than are the literature composites, whereas the flexural strengths are in the intermediate to high end of the literature values. This higher flexural modulus and similar flexural strengths are due to the much higher inorganic contents of the glass fiber/mica ratio composites of this study.

The preceding behavior has been observed in a general sense by other researchers. Inubushi et al. studied mica–epoxy composites with mica loadings in the range of 0–0.15 volume fraction and found that as more mica was added to the epoxy the flexural modulus increased.[21] For resins and mica diameters similar to the present composites, a linear increase in the flexural modulus was observed, but no attempt was made to explain this behavior. Furthermore, the addition of mica was found to significantly lower the flexural strength. Newaz studied clay–polyester composites with clay loadings up to 10 vol % and found that the addition of clay particles increased the tensile modulus and decreased the tensile strength and strain.[22] Although neither Inubishi et al. nor Newaz found the same specific relationship as in the present study, this would not be expected since the composite system currently being studied contains both glass fibers and mica at significantly higher loadings. Nonetheless, their observations appear to hold for the current systems, that is, the addition of inorganic fillers tends to embrittle the polymer, creating a stiffer material while at the same time lowering the strength and strain at failure. This behavior is clearly illustrated in the load-deflection curves shown in Figure 11.

Acoustic Emission during Flexural Deformation

Prefailure Analysis as a Function of Composition

The prefailure damage mechanisms of these composites were investigated using AE. Two approaches were used in this study. The first involves monitoring the amplitude distributions as a function of composition and is referred to as a compositional analysis. The second involves monitoring the damage accumulation as a function of amplitude region for the different compositions and is referred to as an amplitude analysis.

Figure 12 shows the result of the compositional analysis. It is worthy to note that all the AE data is typical, in that at least three samples were run per composition. The amplitude distribution of the all-mica composite, shown in Figure 12(A), has only one peak starting at about 25 db and ending at 42

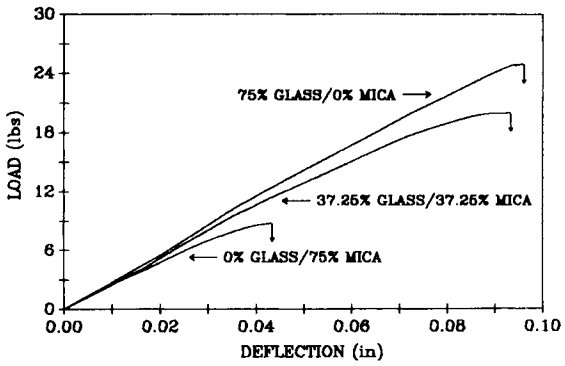

Figure 11 Flexural load-deflection curves.

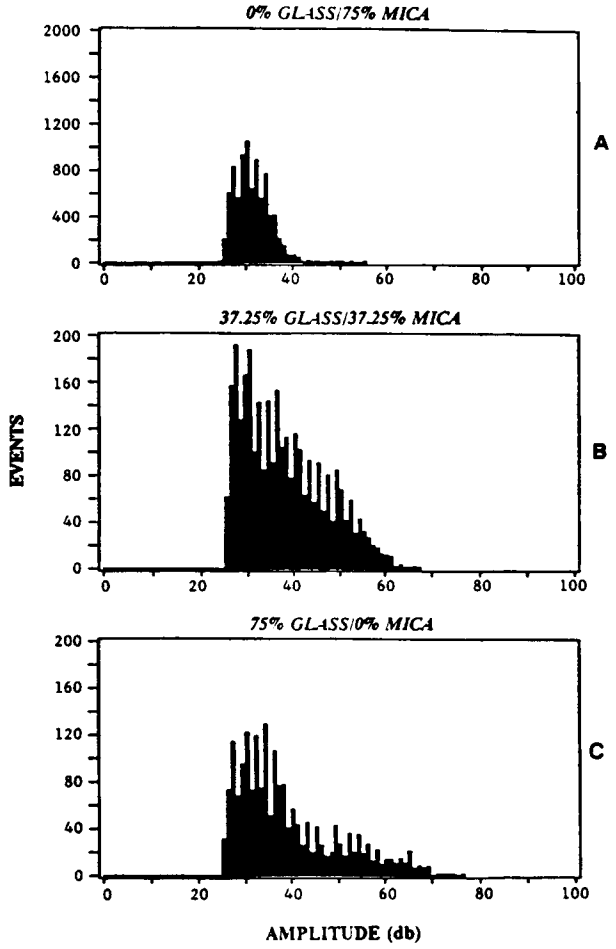

Figure 12 Compositional analysis of the composites showing their AE fingerprint.

db. This indicates that only one damage mechanism, detectable by AE, is occurring. There are two possible damage mechanisms: matrix cracking or epoxy–mica debonding. This amplitude distribution is designated "low amplitude" and includes all events from 0 to 42 db. As soon as glass fibers are added to the composition, three amplitude peaks occur, as seen in Figure 12(B). This indicates that the glass fibers must be causing these new damage mechanisms. As previously stated, the possible damage mechanisms associated with glass fibers are fiber fracture or interfacial debonding. It therefore follows that fiber fracture and/or interfacial debonding are causing the "high-amplitude" distribution, which is taken from 43 to 100 db for analytical purposes. This amplitude range has been associated with these mechanisms by other researchers.[2,17,18] Figure 12(C) shows the amplitude distribution for the all-glass fiber composite. It too shows three amplitude peaks, similar to the 37.25/37.25 composite in that the same range of events occurs. Since the low-amplitude events in the distribution are still present, they must be due to matrix cracking and not to epoxy–mica debonding. Other researchers have associated low-amplitude events with matrix cracking.[2,4,17,18,23]

Damage Analysis by Amplitude Segregation

Figure 13 shows the accumulation of the low-amplitude events as a function of composition. The 0/75 composition, shown in Figure 13(A), exhibits a constant increase in the rate of damage accumulation to failure. The occurrence of low-amplitude events throughout the deformation process has been observed by others.[4,24] Note also that the damage starts in the linear region, which for this composite ends at about 0.12% strain. Damage in the linear

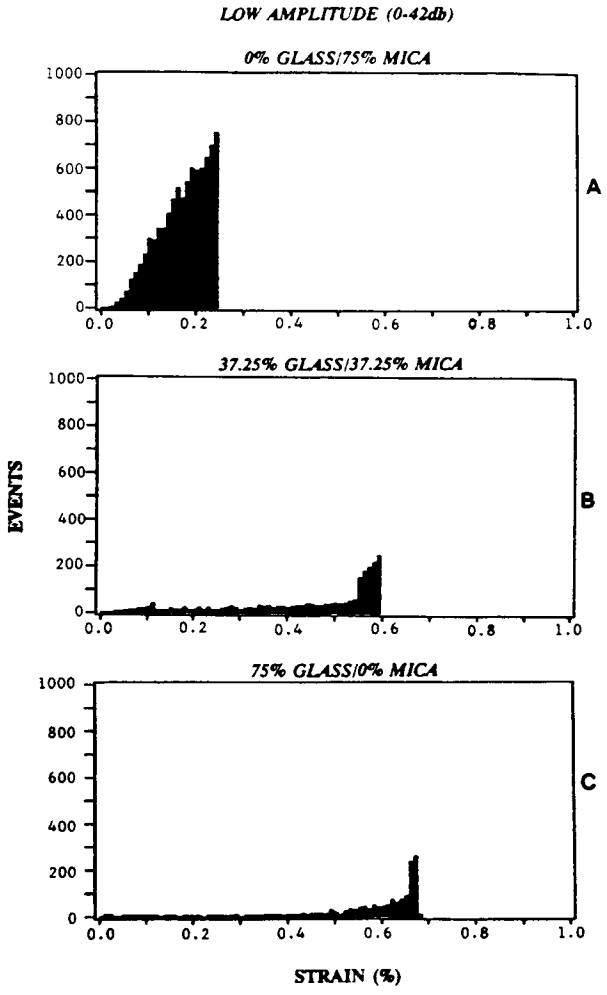

Figure 13 Amplitude analysis of the composites showing the low-amplitude (0–42 db) events vs. strain.

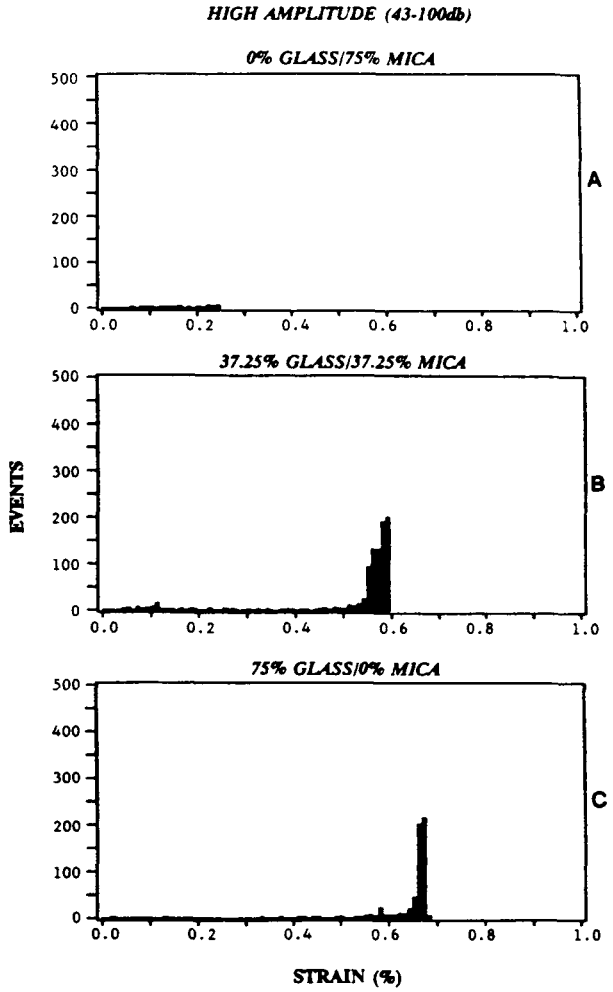

Figure 14 Amplitude analysis of the composites showing the high-amplitude events (43–100 db) vs. strain.

region has been observed before.[18] Again, the addition of glass fibers has a profound effect on the low-amplitude AE damage accumulation behavior. The 37.25/37.25 composition, shown in Figure 13(B), also exhibits AE in the linear region, which ends at about 0.22% strain. However, the AE accumulates at a constant rate until just prior to failure where there is a rapid increase in the last 0.05% strain. The all-glass composite, shown in Figure 13(C), exhibits very little AE activity in the linear region, which ends at approximately 0.28% strain, and a somewhat more gradual AE activity at higher strains. However, the rapid increase in events still occurs just prior to failure in the last 0.03% strain.

Figure 14 shows the damage accumulation related to the high-amplitude events. By definition of the low-amplitude region, no high-amplitude events occur in the 0/75 composite, as shown in Figure 14(A). Figure 14(B) shows the accumulation in the 37.25/37.25 composite. An insignificant number of events occurs until just prior to failure, at which point the number of events increase rapidly. This occurs in the same region as the rapid increase of low-amplitude events. Other researchers have observed a rapid increase in high-amplitude events just prior to failure.[4,24] The all-glass-fiber composite, shown in Figure 14(C), exhibits the same behavior as does the 37.25/37.25 composition in that an insignificant number of events occurs until just prior to failure, at which point the number of events increases rapidly.

The preceding AE analysis suggests that the low-amplitude events are due to matrix cracking whereas the high-amplitude events are due to fiber breakage and/or fiber–matrix debonding. Also, the all-mica composite exhibits substantially different damage accumulation than do the composites that contain glass fibers. Although this analysis has proven beneficial, some questions remain such as what specific mechanism is causing the high-amplitude events and

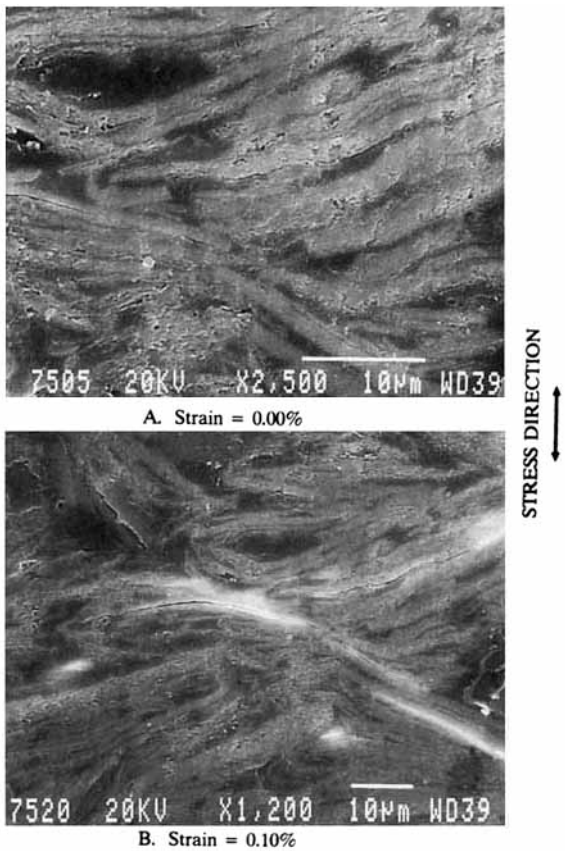

Figure 15 Crack initiation in the 0% glass/75% mica composite.

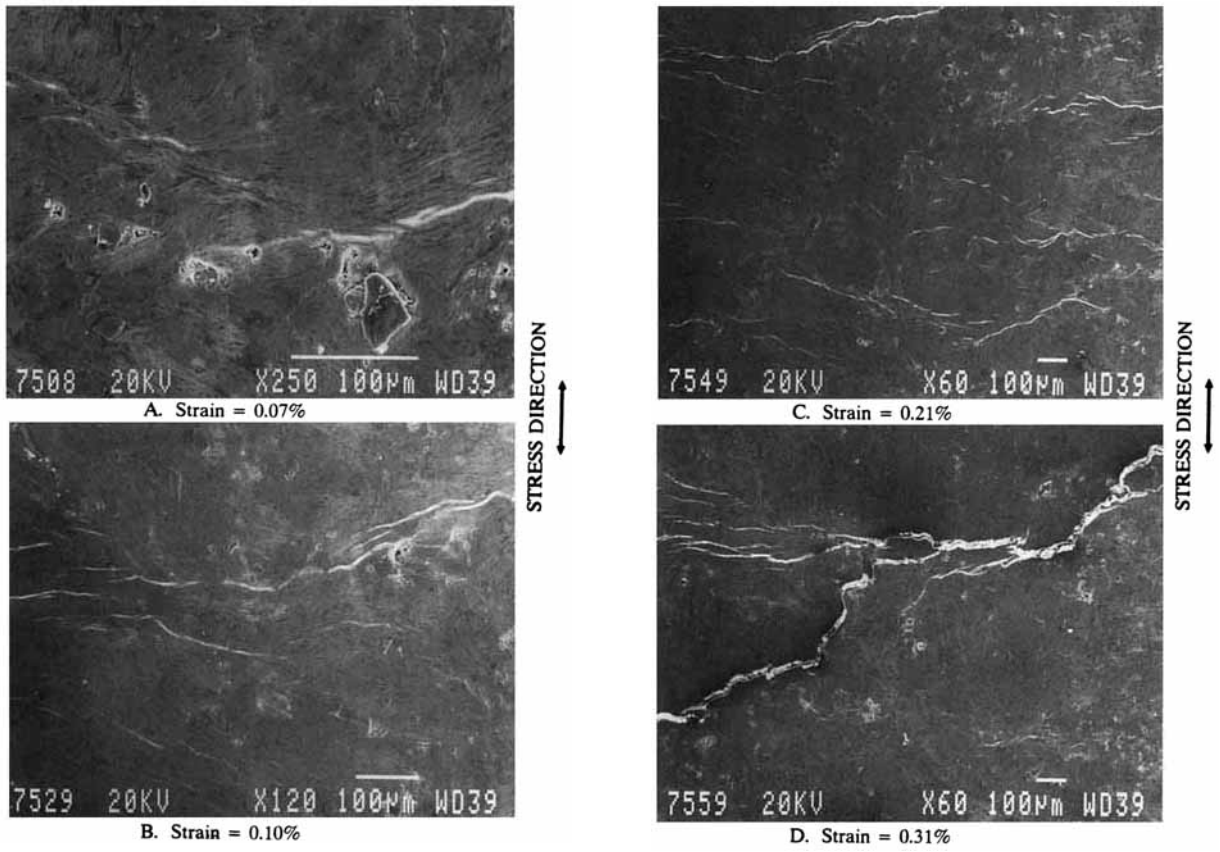

Figure 16 Damage sequence of the 0% glass/75% mica composite.

what exactly is the nature of the damage accumulation. This is the impetus behind coupling AE with other techniques, such as SEM.

Scanning Electron Microscopy during Flexural Deformation

To answer the questions just raised and to further confirm the AE suggested mechanisms, *in situ* SEM observations were conducted on the composites using the apparatus shown in Figure 2 with the technique described in the Experimental section. This technique allows observation of the damage processes on the tensile side of the flexure sample as a function of strain, which can then be correlated to the AE data.

0% Glass/75% Mica Composite

Figure 15 shows the initiation of damage in the all-mica composite. In the unstrained micrograph, Figure 15(A), the presence of microcracks on the order of 10 microns is seen to exist at what appears to be the mica interface. These are most likely due to thermally induced stresses arising during the curing process, in which the cracks would preferentially form at the mica interface because of the poor mica adhesion. Microcracks initiate at these preexisting flaws at strains in the range of 0.10%, which is still in the linear region. This is consistent with the fact that AE is detected in the linear region.

Figure 16 shows the damage sequence for this composite. Once the microcracking has initiated, it tends to follow the mica interface with additional propagation through the matrix as shown in Figure 16(A), in a direction roughly perpendicular to the applied stress. This would be expected since the mica has a much higher strength than does the epoxy.[25] Upon increasing strain, numerous cracks are observed as indicated in Figure 16(B), which has a lower magnification than does Figure 16(A). These cracks continue to grow and coalesce, as shown in Figure 16(C), until final failure occurs as shown in Figure 16(D). This mechanism correlates well with the AE data of Figure 13(A), which shows a constant increase in the rate of damage accumulation to failure, as there is a rapid proliferation of damage

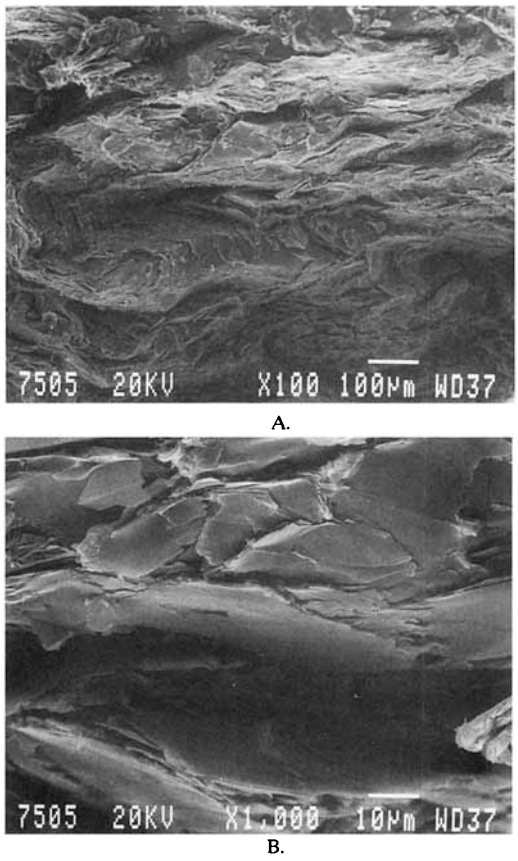

Figure 17 Fracture surfaces of the 0% glass/75% mica composite at 100× (A) and 1000× (B) magnification.

observed in the SEM as the strain increases. Furthermore, only one mechanism is observed in the SEM, which confirms the interpretation of the AE compositional analysis of Figure 12.

Figure 17 shows the fracture surface of the all-mica composite. The fracture surface at high magnification, Figure 17(A), is relatively smooth when compared with the fracture surfaces of the composites that contain glass. This indicates a brittle type of fracture, which is in agreement with the literature citing the embrittlement of epoxies by the addition of mica. Figure 17(B) shows that the mica appears to be oriented in a perpendicular direction to the plane of fracture (i.e., parallel to the composite surface). Furthermore, the mica flakes are very smooth, indicating poor adhesion to the epoxy. This supports the observation that crack initiation starts at the preexisting flaws at the mica interface as the particles act as stress concentrators during the curing process. Because of poor adhesion of the mica to the epoxy, debonding occurs at the interface creating the preexisting flaws.

37.25% Glass/37.25% Mica Composite

As was seen in the AE analysis, as soon as glass fibers were added to the composition, the amplitude distribution as well as the damage accumulation changed dramatically. Figure 18 shows the initiation of the damage between 0.06 and 0.12% strain at what appears to be the mica particles. Even though the coating has broken at 0.06% strain, this does not necessarily mean the crack has grown, as it is likely that this was a site of a preexisting microcrack. However, the crack has most definitely grown from 0.06 to 0.12% strain, which is still well within the linear limit of 0.22% strain. This confirms the AE that showed the occurrence of damage in this region.

The damage sequence of this composite, as the AE has indicated, is very different from the all-mica composite. Figure 19(A) shows the initial damage that was shown at much higher magnification in Figure 18. The observed cracks do not grow substantially until much higher strains, as illustrated in Figure 19(B), which is already at 0.49% strain. At these strains, evidence of fiber breakage and fiber

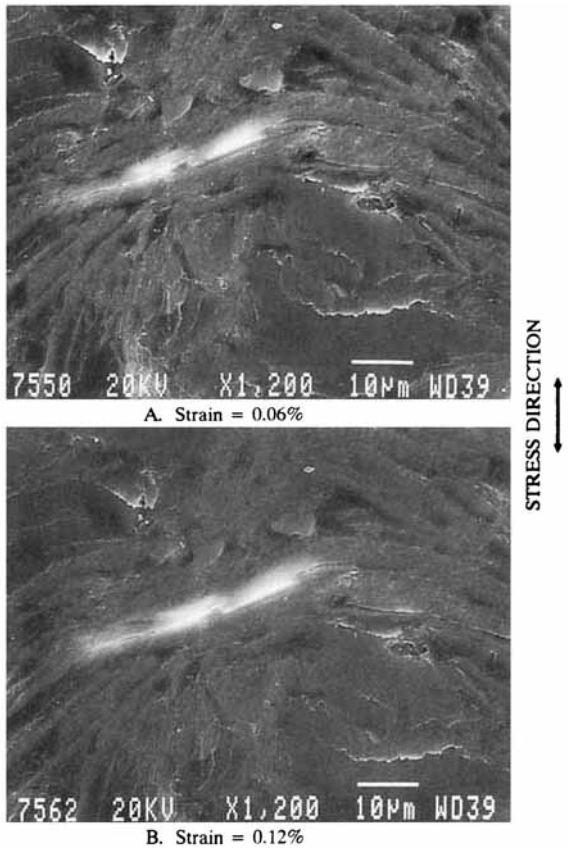

Figure 18 Crack initiation in the 37.25% glass/37.25% mica composite.

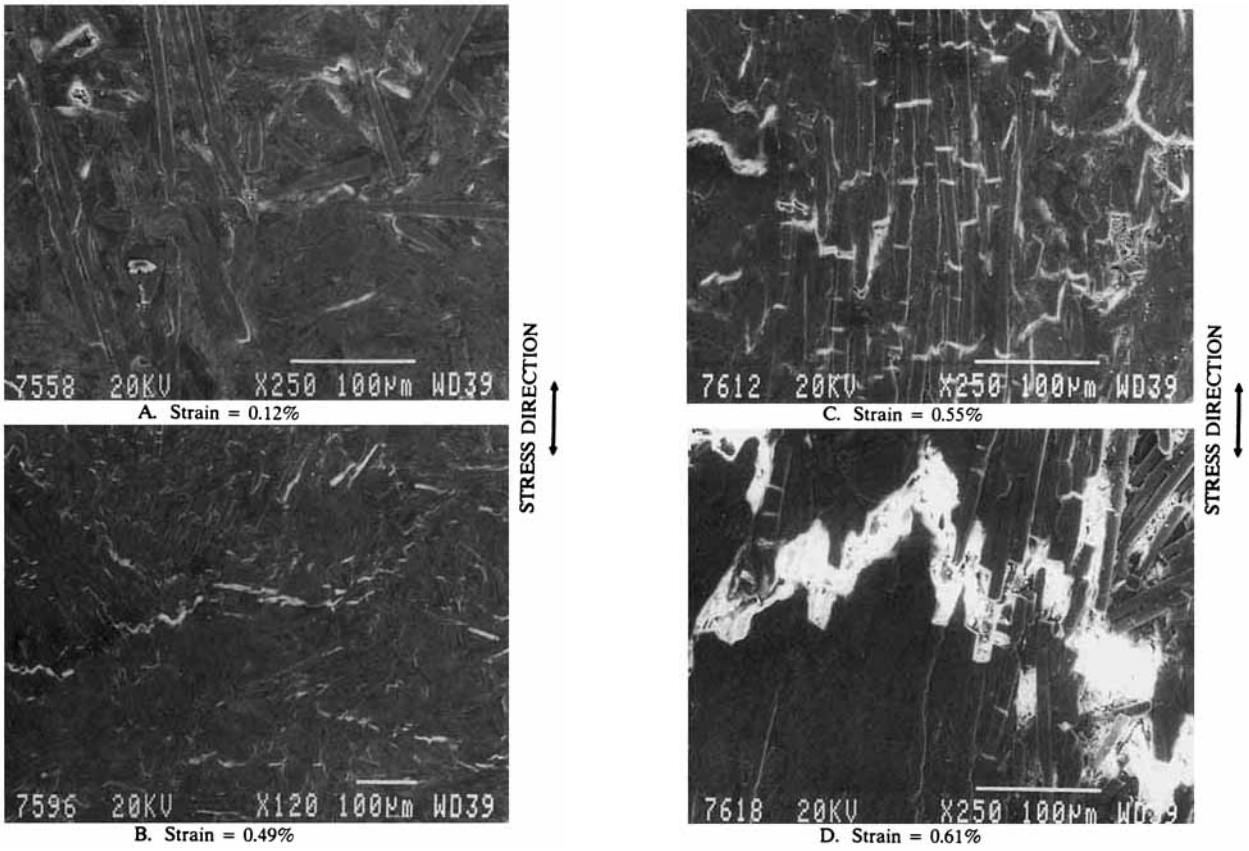

Figure 19 Damage sequence of the 37.25% glass/37.25% mica composite.

debonding is observed. However, because of the polishing required, some of these fibers may have been predamaged. Figure 20, however, clearly shows evidence of fiber breakage at about 0.49% strain. Although this strain level does not correlate exactly to the majority of high-amplitude events shown in Figure 14(B), it is within experimental deviations. Further evidence that debonding and fiber breakage are observed at higher strains, is shown in Figure 19(C), a slightly higher magnification than in Figure 19(B). Figure 19(D), the final macrocrack, clearly shows evidence of fiber pull-out and breakage.

Also evident in the fracture surfaces, shown in Figure 21, are pulled-out fibers. These fibers, unlike the mica particles, are not smooth but have resin remaining on them, indicating good fiber adhesion. Figure 21(B), the surface at higher magnification, shows evidence of cracking along the mica particles. This agrees with the observed crack initiation. Also, when Figure 21(A) is compared with the all-mica composite fracture surface of Figure 17(A), it is clear that the surface of the composite containing glass fibers is much rougher.

75% Glass/0% Mica Composite

The all-glass-fiber composite shows similar behavior to the 37.25/37.25 composite except for the crack initiation. Figure 22 shows the nature of the crack initiation. Evidence of preexisting microcracks in the matrix, as well as voids, is observed, and growth from these sites occurs almost at the linear limit, which is 0.28% strain. This agrees well with the AE accumulation data of Figure 13(C) in which there is little AE activity in the linear region.

The fracture surfaces are shown for the all-glass-fiber composite in Figure 23. Figure 23(A) clearly shows that the fibers are not in a totally random distribution but are in a transversely isotropic orientation. It is also apparent that many pulled-out fibers are present. This is shown close up in Figure 23(B), where it is observed that although some fibers are devoid of resin, most have resin remaining on them, indicating good fiber adhesion. The fibers without resin on them most likely were surrounded by a void as other micrographs showed the presence of voids.

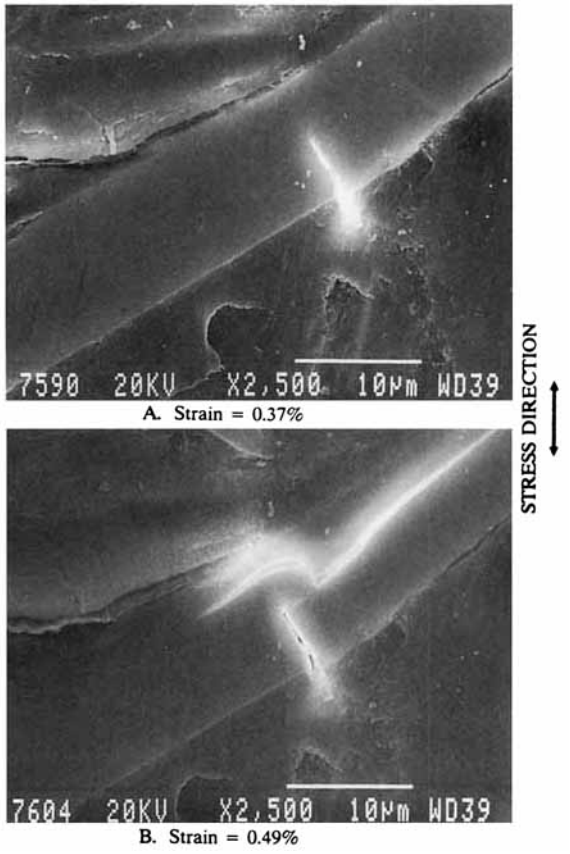

Figure 20 Damage detail of the 37.25% glass/37.25% mica composite.

Prefailure Damage Mechanisms Based on AE Data and SEM Observations

0% Glass/75% Mica Composite

Based on the AE data and the SEM observations, it is possible to develop a damage mechanism. In the all-mica composite, microcracking starts in the linear region at preexisting flaws located at the mica interface as shown in Figure 15. These microcracks grow along the mica contours over the majority of the deformation process, producing low-amplitude events, until final fracture occurs. Fracture occurs at much lower strains than in the glass-containing composites because the mica cannot toughen the matrix as the glass fibers do because of its poor adhesion to the matrix (shown in Fig. 17) as well as its lower aspect ratio.

37.25% Glass/37.25% Mica Composite

In the 37.25/37.25 composite, microcracking starts in the linear region at preexisting flaws located at the mica particles as shown in Figure 18. These microcracks grow slowly, producing low-amplitude events, as the strain increases but are prevented from causing failure at low strains because the glass fibers, due to their good fiber adhesion to the epoxy, toughen the material as indicated in Figures 11 and 13(B and C). Once a critical strain is reached, however, fiber breakage and pull-out are observed as shown in Figures 19 and 20. These mechanisms produce high-amplitude events as shown in Figures 12 and 14(B). At this strain, approximately the last 10% of the failure strain, catastrophic crack growth occurs, producing a rapid increase in both the low- and high-amplitude events and causing ultimate failure.

75% Glass/0% Mica Composite

In the all-glass-fiber composite, microcracking initiates at preexisting flaws and voids instead of at

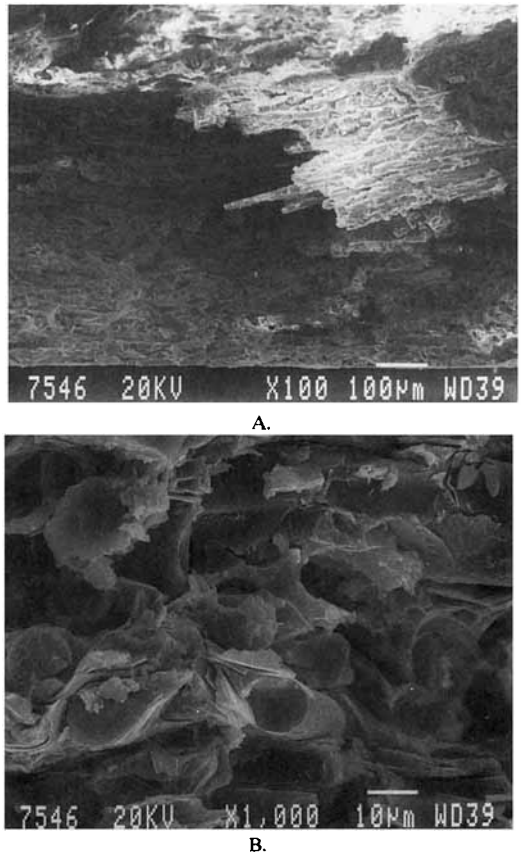

Figure 21 Fracture surfaces of the 37.25% glass/37.25% mica composite at 100× (A) and 1000× (B) magnification.

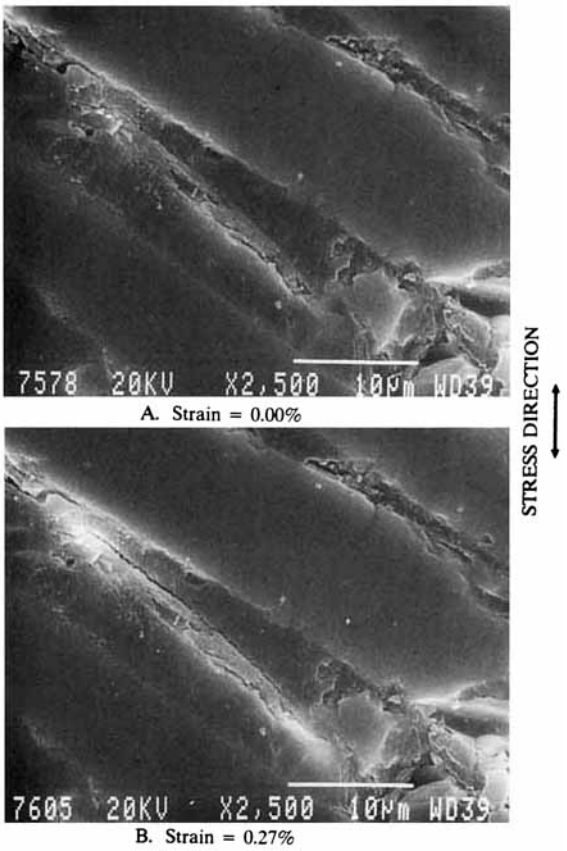

Figure 22 Crack initiation in the 75% glass/0% mica composite.

mica particles as shown in Figure 22. Upon increasing strain, the crack propagates in a similar manner as does the 37.25/37.25 composite up to failure, which occurs at slightly higher strains.

CONCLUSIONS

1. A unique class of highly filled composite materials composed of glass fibers, mica, and epoxy resin have been optimized with respect to flexural properties. Furthermore, as the glass-to-mica ratio was increased, the flexural strength and maximum strain increased while the flexural modulus decreased.
2. Three prefailure damage processes were identified: (a) matrix cracking, which occurred throughout the deformation process and was associated with low-amplitude events, (b) glass fiber pull-out, and (c) glass-fiber breakage, both of which occurred only at high strains and were associated with high-amplitude events.
3. In the all-mica composite, microcracking initiated in the linear region at preexisting flaws, on the order of 10 μm, located at the mica interface. These microcracks grew along the mica contours over the majority of the deformation process, emitting low-amplitude events, until final fracture occurred.
4. In the glass-containing composites, microcracking initiated in the linear region at preexisting flaws and voids, on the order of 10 μm. These microcracks grew slowly, emitting low-amplitude events, as the strain increased but were prevented from causing failure at low strains because of toughening from the glass fibers. At high strains, fiber breakage and pull-out occurred, emitting high-amplitude events. At strains just prior to failure, catastrophic crack growth occurred, producing a rapid increase in both low- and high-amplitude events.

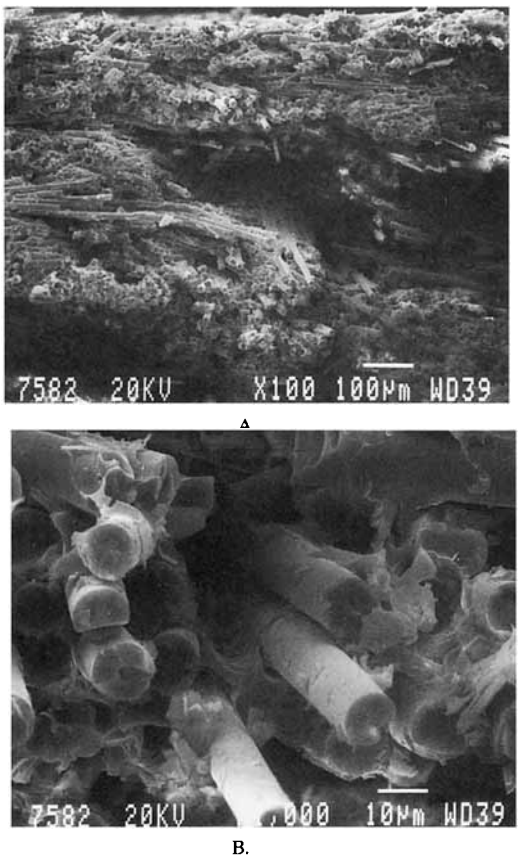

Figure 23 Fracture surfaces of the 75% glass/0% mica composite at 100× (A) and 1000× (B) magnification.

Financial support was provided by the NASA-CCDS Materials for Space Structures.

REFERENCES

1. M. A. Hamstad, *Exp. Mechan.*, **March,** 7–13 (1986).
2. L. Li and J.-H. Zhao, in *2nd International Symposium on AE from Reinforced Composites,* Soc. Plas. Ind., Montreal, Canada, Section 3, 1986, pp. 90–95.
3. N. Sato, T. Kurauchi, and O. Kamigaito, *J. Mater. Sci.,* **21,** 1005–1010 (1986).
4. M. Faudree, E. Baer, and A. Hiltner, *J. Compos. Mater.,* **22,** 1170–1195 (1988).
5. J. M. Berthelot and J. Rhazi, in *2nd International Symposium on AE from Reinforced Composites,* Soc. Plas. Ind., Montreal, Canada, Section 3, 1986, pp. 96–103.
6. Dow Chemical Co., *Dow Liquid Epoxy Resins,* 1988.
7. R. A. Cull, *Space Environment Effects on Elastomeric Materials,* American Chemical Society-Rubber Division, Dallas, TX, April 1988.
8. ASTM-D790M-84.
9. L. A. Carlsson and R. B. Pipes, *Experimental Characterization of Advanced Composite Materials,* Prentice-Hall, Englewood Cliffs, NJ, 1987, pp. 89–90.
10. J. M. Whitney, I. M. Daniel, and R. B. Pipes, *Experimental Mechanics of Fiber Reinforced Composite Materials,* Society for Experimental Mechanics, Prentice-Hall, Englewood Cliffs, NJ, 1984, p. 166.
11. C. B. Scruby, *J. Phys. E. Sci. Instrum.,* **20,** 946–953 (1987).
12. A. A. Pollock, *Practical Guide to Acoustic Emission Testing,* Technical Report #TR-108-3-3/88, Physical Acousics Corp., Princeton, NJ, 1988.
13. J. R. Mitchell, *Plast. Eng.,* **January,** 29–32 (1984).
14. L. Koenczoel, A. Hiltner, and E. Baer, *Polym. Compos.,* **8**(2), 109–114 (1987).
15. I. Narisawa and H. Oba, *J. Mater. Sci.,* **19,** 1777–1786 (1984).
16. R. L. Mehan and J. V. Mullin, *J. Compos. Mater.,* **5,** 266–269 (1971).
17. J. Yuan, A. Hiltner, and E. Baer, *Polym. Compos.,* **7**(1), 26–35 (1986).
18. F. Chen, A. Hiltner, and E. Baer, in *High Temperature Polymers and Their Uses,* Soc. Plas. Eng., Cleveland, OH, Session IV, October 1989, pp. 190–203.
19. J. Rooum and R. D. Rawlings, *J. Mater. Sci.,* **17,** 1745–1752 (1982).
20. D. Valetin, *Composites,* **16**(3), 225–230 (1985).
21. S. Inubushi, T. Ikeda, S. Tazuke, T. Satoh, and Y. Kumagai, *J. Mater. Sci.,* **23,** 1182–1188 (1988).
22. G. M. Newaz, *Polym. Compos.,* **7**(3), 176–181 (1986).
23. H. Otsuka and H. A. Scarton, *J. Compos. Mater.,* **15,** 591–597 (1981).
24. N. Sato, T. Kurauchi, and O. Kamigaito, *J. Compos. Mater.,* **22,** 447–458 (1988).
25. J. E. Gordon, *The New Science of Strong Materials,* Princeton University Press, Princeton, NJ, 1984, pp. 121–122.

Received July 12, 1990
Accepted August 15, 1990